Wireless Powered Cognitive Radio Networks with Multiple Antenna Sources and Hardware Impairments

Addanki Prathima[a], Devendra S. Gurjar[a,*], Yuming Jiang[b], Suneel Yadav[c]

[a]*Department of Electronics and Communication Engineering, National Institute of Technology Silchar, Assam, 788010, India*
[b]*Department of Information Security and Communication Technology, Norwegian University of Science and Technology (NTNU), NO-7491 Trondheim, Norway*
[c]*Department of Electronics and Communication Engineering, Indian Institute of Information Technology, Allahabad 211012, India*

Abstract

In this paper, a radio-frequency (RF) energy harvesting enabled cognitive radio network (CRN) is considered in the presence of transceiver hardware impairments (HIs). Herein, one of the secondary nodes (SNs) exploits simultaneous wireless information and power transfer (SWIPT) technology to harvest energy from the primary signal and provides relay assistance for the primary transmission. We consider multiple antennas at the primary nodes (PNs) to ensure better link reliability and spectrum sharing to mitigate the spectrum scarcity. In the first phase, relaying SN uses non-linear energy harvester circuit to harvest energy from the received RF signals from PN based on the power splitting approach. In the second phase, the same SN adds its own signal intended for other SN along with the primary signal and broadcasts the combined signal. Assuming the network to operate in a Nakagami-m fading environment, the performance of the considered CRN is evaluated in terms of outage probability (OP) and system throughput. Also, we formulate two optimization problems to minimize the OP and maximize the system throughput. The Karush-Kuhn-Tucker conditions are used to obtain the closed-form solution of the constrained convex optimization. Numerical results are provided to examine the perfor-

*Corresponding author.
Email address: dsgurjar@ece.nits.ac.in (Devendra S. Gurjar)

mance impact concerning different system and channel parameters.

Keywords: Cognitive radio network, hardware impairments, Nakagami-m fading, non-linear energy harvester, outage probability, SWIPT.

1. Introduction

Spectrum sharing has become inevitable in the current wireless communication technology due to the rapid increase in the number of wireless connected devices and the consequent huge demand of the fixed spectrum [1]. Thus, the cognitive radio has emerged as a promising solution to combat spectrum congestion issues. Among the three popular spectrum sharing schemes in literature [2], i.e., underlay, overlay, and interweave, the overlay spectrum sharing scheme provides relay assistance to the primary system in the allocated duration over the same licensed spectrum band. Another key constraint in wireless networks is the network lifetime. Recent works have shown that radio-frequency (RF) signals can carry both information and power simultaneously [3]. Therefore, receiver with appropriate circuitry [4] to enable simultaneous wireless information and power transfer (SWIPT) technology, can decode information as well as harvest energy from the RF signal which can help in increasing the network lifetime. Based on the literature, SWIPT in receiver design can be implemented using three popular techniques, i.e., time switching (TS), power splitting (PS), and antenna switching (AS) [5]. Among these three receiver designs, PS enabled SWIPT exhibits superior performance as compared to other SWIPT techniques [6]. Therefore, PS-based SWIPT is adopted in this paper for energy harvesting. The receiver circuit enabled with RF energy harvesting comprises of non-linear elements such as diodes, capacitors and inductors and hence, a non-linear energy harvesting (EH) model with two segments [7] is considered for a more realistic approach.

Another critical aspect of cooperative communication is to ensure transmission reliability. The adversities at the terminal nodes and physical layer security issues may cause hindrance to the transmission of primary signals [8]. There-

fore, providing diversity using multi-antenna techniques ameliorates the aforementioned problems and aids in establishing a reliable transmission link while providing improved signal transmission rates [9]. Also, the RF transceivers are associated with various hardware imperfections [10] which limit the system performance. Hence, considering these hardware impairments (HIs) in multi-antenna techniques makes it a more practical approach towards analyzing the system performance.

1.1. Prior Works

In the recent past, many researchers have worked on wireless energy harvesting in cooperative communication networks [11, 12, 13, 14, 15, 16, 17]. The authors in [11] have proposed a SWIPT enabled spectrum sharing scheme and determined the optimal power allocation to maximize the system throughput while maintaining the quality-of-service (QoS) of the primary system. In [12], the authors have proposed an energy-assisted decode-and-forward (DF) protocol to address the issue of energy scarcity and spectrum scarcity, and have conducted a comprehensive analysis of the proposed protocol with conventional amplify-and-forward (AF) and DF protocols. In [13], an overlay spectrum sharing scheme is studied for the outage performance of the system under Nakagami-m fading. In [14], the performance of SWIPT in cognitive radio networks (CRNs) with AS technique is investigated for Rayleigh and Nakagami-m fading channels. Different from the above works, the authors in [15] have studied opportunistic relaying with dynamic energy harvesting scheme. Ambient backscatter communication is adopted in [16] integrated with SWIPT based CRN to improve the network performance in terms of system throughput and energy efficiency. Likely, the outage performance of an underlay CRN has been studied in [17]. Assuming, opportunistic spectrum access and sensing-based spectrum sharing, the authors in [18] have studied a wideband SWIPT-based cognitive radio with imperfect channel state information (CSI) and spectrum sensing. In [19], the outage performance of an EH based bidirectional CRN is studied assuming DF relaying protocol. Further, in [20], the authors have studied a SWIPT-

based CRN for relay selection problem by adopting data-driven relay selection strategies. The work in [21] addressed resource allocation issues in a two-tier primary–secondary network and formulated an optimization problem for maximizing secondary user throughput with a constraint on primary throughput. In [22], the authors studied a joint meta-heuristic approach of particle swarm optimization cuckoo search algorithm for resource allocation problem in wireless powered CRN-SWIPT framework in Rayleigh fading environment. The authors in [23] investigated security aspects in a non-ideal transceiver relaying network and presented a joint optimization of relay beamformer and transmit powers to maximize the average secrecy rate. Recently in [24], the authors formulated a throughput maximization-based resource allocation scheme for a wireless powered hybrid backscatter-active communication network while considering transceiver hardware impairments.

Recently, beamforming in SWIPT enabled wireless networks have gained much attention due to better transmission reliability, increased power and information transfer efficiency [25]. Works in [26]-[27] have adopted beamforming in SWIPT based CRNs. In particular, research work in [26] have proposed an overlay spectrum sharing scheme for improving rate and error performance. In [28], the authors have considered a multi-user multiple-input-single-output (MISO) CRN coupled with PS-SWIPT under the criteria of fairness of users' harvested energy, worst-user harvested energy-interference power and derived the closed form solutions for transmit power minimization and EH maximization. For a similar network in [29], the authors have investigated for secure communication with robust beamforming under imperfect CSI. In [30], the authors have considered a PS SWIPT-aided multiuser MISO underlay CRN with the aim to minimize the secondary transmit power by jointly optimizing the transmit beamforming vector and the PS ratios satisfying the required EH and QoS and interference constraints. While in [27], the authors have addressed the issue of receive beamforming, joint transmit beamforming and power allocation in similar network. In [31], the outage performance and ergodic sum rate are obtained for a two-way relay network (TWRN) with multiple antenna sources

and channel estimation errors. In [32], the authors have considered a full-duplex TWRN with multiple antennas at the source nodes and a pair of antennas at the relay node, and analyzed the outage performance, diversity order under antenna selection strategy. In [33], the authors have studied the problem of minimizing the total power consumption by exploiting a beamforming scheme in an untrusted underlay CRN. The authors in [34] have studied the performance of amplify-forward relaying in dual-hop configuration with hardware impairments. Research work in [35] investigates optimal power allocation scheme in an IoT system with decode-and-forward relaying while considering transceiver hardware impairments. The authors in [36] have studied the performance of a two-way AF relaying system in the presence of hardware impairments over Nakagami-m fading channels and derived closed-form expressions for the outage probability, ergodic capacity and asymptotic symbol error rate. In [37], the authors have considered a SWIPT-based CRN with multiple antennas at the secondary node and studied the joint beamforming and relay selection problem for the same. Similarly, in [38], a TWRN with multiple antennas at the cognitive transmitter is designed for secure cooperative transmission and the secrecy sum rate is maximized.

In this work, we are interested in exploring a robust SWIPT-based CRN model with overlay strategy towards improving the link reliability while adopting a more practical approach in the system design considerations. As a sequence, primary nodes are equipped with multiple antennas to enhance the link reliability. To make the system more practical, the distortion noise caused due to HIs is taken into account at all the nodes. Also, a more realistic non-linear model is adopted for energy harvesting. However, with all the above considerations, the system performance highly depends on the spectrum sharing and PS factors. This facilitates the need to optimize the system design parameters to attain optimal system performance. With this motivation, we investigate the impact of HIs on the system performance of primary and secondary links and disclose the ceiling effects. Moreover, we deduce an approach for effective spectrum sharing at the secondary node and optimize the system parameters

to achieve minimal outage probability at the primary node and maximal overall system throughput while maintaining the QoS at the primary terminals. To the authors' best knowledge, no work has yet analyzed the performance impact of HIs on SWIPT-based CRN with a non-linear PS energy harvester circuit and multi-antenna primary transceivers over the Nakagami-m fading channels.

1.2. Major Contributions

Motivated by the above discussion, in this paper, we consider an RF energy harvesting enabled CRN to tackle two fundamental challenges of wireless networks, viz., network lifetime and spectrum scarcity. The secondary nodes use the harvested energy to facilitate relay assistance to the primary nodes while realizing their communication. The system is modeled and studied so that it maintains the QoS at the PNs. Also, we take into account the presence of HIs to give more practical insights concerning such futuristic complex wireless systems. For analysis of the system performance, we proficiently obtain expressions of the outage probability (OP) and system throughput over Nakagami-m fading by considering multiple antennas at the PNs and the presence of HIs. In order to determine the optimal system design parameters in compliance with the above-mentioned considerations, we formulate two optimization problems, viz., outage probability minimization, and system throughput maximization. The significant contributions in this paper can be summarized as follows.

- This paper characterizes the modeling of HIs in a non-linear EH-based PS-SWIPT CRN with multiple antenna sources at the primary end. In this outline, we derive the instantaneous signal-to-noise and distortion ratio expressions at both primary and secondary nodes.

- Assuming the system to operate under Nakagami-m fading environment, we derive the expressions for OP of both primary and secondary links. Subsequently, we obtain the system throughput, which is a significant performance metric in this work. Asymptotic OP analysis is also conducted in the high SNR region to get valuable insights into the system

performance.

- We investigate the considered system scheme for system spectrum ceiling and overall system ceiling effects under the impact of HIs to ensure the primary link is not in outage. Also, effective spectrum sharing at the SN is taken care of by determining the feasible range of the spectrum sharing factor.

- We optimize two non-linear programming problems for minimizing primary outage probability and maximizing the system throughput. They are proved to be convex functions and hence solved using Karush-Kuhn-Tucker (KKT) conditions to obtain the corresponding optimal PS and spectrum sharing factors.

- Extensive analytical and simulation results are presented to give significant insights into the system behavior and its performance measures concerning various system and channel parameters.

Notations: $\Pr[\cdot]$, $f_X(\cdot)$, and $F_X(\cdot)$ denote respectively the probability, probability density function (PDF) and the cumulative distribution function (CDF) of a random variable X. The upper incomplete, the lower incomplete, and the complete gamma functions are represented as $\Gamma[\cdot,\cdot]$, $\Upsilon[\cdot,\cdot]$, and $\Gamma[\cdot]$, respectively [39, eq. (8.350)]. $\mathcal{K}_v(\cdot)$ represents vth order modified Bessel function of second kind [39, eq. (8.432.1)] and $\mathcal{W}_{u,v}[\cdot]$ denotes Whittaker function [39, eq. (9.222)].

2. System Model

As depicted in Fig. 1, the considered CRN consists of two primary nodes $\mathsf{PN_a}$ and $\mathsf{PN_b}$, and a pair of secondary nodes $\mathsf{SN_t}$ and $\mathsf{SN_r}$. Here, nodes $\mathsf{PN_a}$ and $\mathsf{PN_b}$ are equipped with $\mathsf{N_a}$ and $\mathsf{N_b}$ number of antennas, respectively, and SNs are equipped with single antennas. It is assumed that the direct link between PNs is not good enough to support the desired rate due to heavy shadowing or blockage. Therefore, we adopt an overlay relaying scheme where $\mathsf{SN_t}$ acts as a

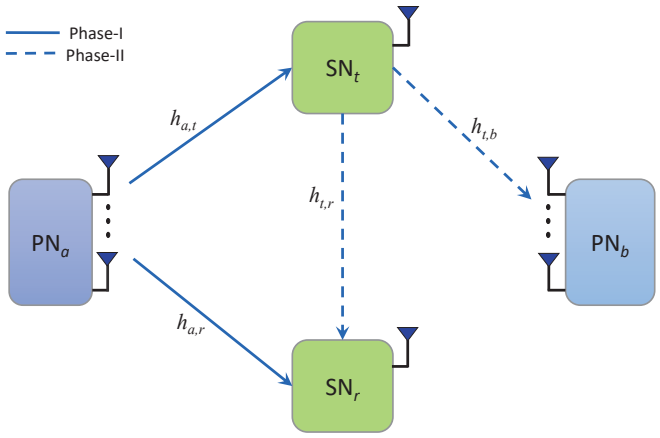

Figure 1: System model of SWIPT-enabled CRN.

relay node to assist the primary transmission. In return to the relay assistance provided by the secondary node, $\mathsf{SN_t}$ is allowed to exchange its own information to the other secondary node $\mathsf{SN_r}$ over the same licensed spectrum. This relaying node $\mathsf{SN_t}$ is enabled with a non-linear energy harvester in order to harvest energy from the signal received from $\mathsf{PN_a}$ using PS technique. All the nodes are assumed to operate in half-duplex mode. The information transmission from $\mathsf{PN_a}$ to $\mathsf{PN_b}$ for one block of duration T is depicted in Fig. 2. One transmission block is divided into two equal phases i.e., each of duration $T/2$. In the first phase, $\mathsf{PN_a}$ transmits signal to $\mathsf{SN_t}$ and $\mathsf{SN_r}$, and some part of the received signal at $\mathsf{SN_t}$ is utilized to harvest energy using PS technique. In the second phase, $\mathsf{SN_t}$ appends the received signal from $\mathsf{PN_a}$ with its own signal and applies DF scheme to broadcast the combined signal. All the channel coefficients are assumed to follow Nakagami-m fading and remain unchanged for one block duration T. The channel vectors between $\mathsf{PN_a}$ to $\mathsf{SN_t}$ and $\mathsf{SN_t}$ to $\mathsf{PN_b}$ are denoted as $\boldsymbol{h}_{a,t} = [h_a^1\, h_a^2 \ldots h_a^{N_a}]^T$ and $\boldsymbol{h}_{t,b} = [h_b^1\, h_b^2 \ldots h_b^{N_b}]^T$, respectively. All the entries of the channel vectors $\boldsymbol{h}_{a,t}$ and $\boldsymbol{h}_{t,b}$ follow Nakagami-m distribution with average power Ω_{at} and Ω_{tb}, and fading severity parameter m_{at} and m_{tb}, respectively.

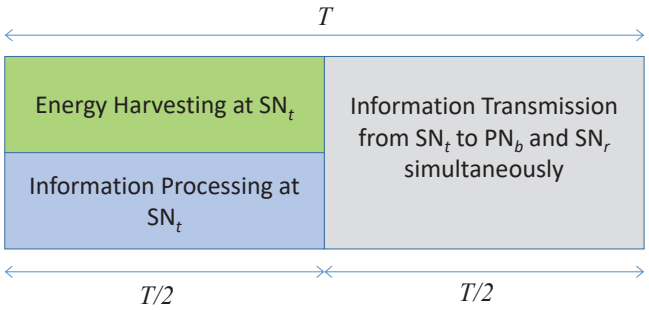

Figure 2: Frame structure for one block duration.

2.1. Signal Modeling with HIs

Practical hardware circuits suffer from impairments such as amplifier non-linearity, in-quadrature-phase (IQ) imbalances, and phase noises, hence causing performance degradation in communication systems [40]. Thus, assuming hardware impairments in transceiver equipment, the received signal can be modeled as [41]

$$y_{pq} = h_{pq}(x_t + \eta_{tp}) + \eta_{rq} + n_q, \tag{1}$$

where h_{pq} is the channel coefficient between two arbitrary communicating nodes P and Q, and P transmits a symbol x_t to Q. y_{pq} denotes the received signal at node Q. $n_q \sim \mathcal{CN}(0, \sigma_q^2)$ is the additive white Gaussian noise (AWGN) component at node Q, η_{tp} and η_{rq} denote the distortion noises due to transceiver impairments where $\eta_{tp} \sim \mathcal{CN}(0, k_t^2 P)$ and $\eta_{rq} \sim \mathcal{CN}(0, k_r^2 P|h_{pq}|^2)$, with $P = \mathbb{E}\{|x_t|^2\}$. k_t and k_r are the parameters that denote the impairments level and can be measured as error vector magnitudes. The overall distortion noise power due to transceiver HIs can be given as

$$\mathbb{E}\{|h_{pq}\eta_{tp} + \eta_{rq}|^2\} = P|h_{pq}|^2(k_t^2 + k_r^2). \tag{2}$$

Using (2), we can express (1) as

$$y_{pq} = h_{pq}(x_t + \eta_{pq}) + n_q, \tag{3}$$

where $\eta_{pq} \sim \mathcal{CN}(0, k^2P)$ is the distortion noise with $k = \sqrt{k_t^2 + k_r^2}$ consisting of both transmitter and receiver impairment levels. It is assumed that all the nodes are equipped with the same hardware circuitry. When $\eta_{pq} = 0$, i.e., the communicating nodes hardware is ideal, the above equation (3) takes the form of conventional model. For ease of analysis, in this work we assume that the HIs level at all nodes are equal and is denoted by k.

2.2. Signal-to-Noise and Distortion Ratio (SNDR)

The signal received from primary node $\mathsf{PN_a}$ at $\mathsf{SN_t}$ in the first phase is divided into two parts using the PS factor β, where β fraction of power is used for EH while the remaining power, i.e., $1-\beta$, is used for information processing (IP). Thereafter, the primary and secondary signals are combined at $\mathsf{SN_t}$ using the spectrum sharing factor α, where α amount of transmit power at $\mathsf{SN_t}$ is allocated for primary signal transmission and the remaining $(1-\alpha)$ power is used for secondary signal transmission.

In the first phase, primary node $\mathsf{PN_a}$ transmits its signal using the transmit beamforming weight vector $\widehat{\mathbf{w_a}}$. Hence, the signal received at the secondary node $\mathsf{SN_t}$ in the presence of HIs is expressed as

$$y_{a,t} = \boldsymbol{h}_{a,t}^T \widehat{\mathbf{w_a}}(x_a^{\mathrm{I}} + \eta_{at}) + n_t, \tag{4}$$

where x_a^{I} is the symbol transmitted by $\mathsf{PN_a}$ in the first phase with power $\mathbb{E}\{|x_a^{\mathrm{I}}|^2\} = P_a$. The $N_a \times 1$ transmit weight vector $\widehat{\mathbf{w_a}}$ for maximum ratio transmission is chosen as [42] $\widehat{\mathbf{w_a}} = \left(\frac{\boldsymbol{h}_{a,t}^\dagger}{\|\boldsymbol{h}_{a,t}\|}\right)^T$. $\eta_{at} \sim \mathcal{CN}(0, k^2P_a)$ is the distortion noise power with $k = \sqrt{k_a^2 + k_t^2}$ and $n_t \sim \mathcal{CN}(0, \sigma_t^2)$ is the AWGN component at $\mathsf{SN_t}$. This received signal at $\mathsf{SN_t}$ is subject to energy harvesting using PS circuit with PS factor β. Thus, $(\sqrt{\beta}y_{at})^2$ power is used for EH while the remaining $(\sqrt{1-\beta}y_{at})^2$ power is utilized for information processing and transmission. The harvested energy E_h at $\mathsf{SN_t}$ is given as

$$E_h = \beta\eta|\boldsymbol{h}_{a,t}^T\widehat{\mathbf{w_a}}|^2 P_a \frac{T}{2}, \tag{5}$$

where η is the energy conversion efficiency and $0 < \eta < 1$. Considering a non-linear EH receiver as in [7], the total harvested power at $\mathsf{SN_t}$ is given as

$$P_h = \begin{cases} \beta\eta P_a \|\boldsymbol{h}_{a,t}\|^2 & \text{for} \quad P_a\|\boldsymbol{h}_{a,t}\|^2 \leq P_{\text{th}} \\ \beta\eta P_{\text{th}} & \text{for} \quad P_a\|\boldsymbol{h}_{a,t}\|^2 > P_{\text{th}}. \end{cases} \tag{6}$$

P_{th} is the saturation threshold power of the energy harvester circuit. Using (4), the remaining received signal at $\mathsf{SN_t}$ for information processing can be expressed as

$$y_{a,t}^{\text{IP}} = \sqrt{1-\beta}(\boldsymbol{h}_{a,t}^T \widehat{\mathbf{w_a}}(x_a^I + \eta_{at}) + n_t) + n_{cr}, \tag{7}$$

where $n_{cr} \sim \mathcal{CN}(0, \sigma_{cr}^2)$ represents the RF to base-band conversion noise at $\mathsf{SN_t}$. Hence, the instantaneous SNDR at $\mathsf{SN_t}$ can be represented as

$$\gamma_{a,t} = \frac{(1-\beta)P_a\|\boldsymbol{h}_{a,t}\|^2}{(1-\beta)k^2 P_a\|\boldsymbol{h}_{a,t}\|^2 + (1-\beta)\sigma_t^2 + \sigma_{cr}^2}. \tag{8}$$

From (8), the instantaneous rate achieved at the information receiver at node $\mathsf{SN_t}$ is $\mathcal{R}_{a,t} = \frac{1}{2}\log_2(1+\gamma_{a,t})$. Now, $\mathsf{SN_t}$ combines the received primary signal and its own signal and broadcasts the resulting signal. $\mathsf{SN_t}$ allocates α fraction of its total transmit power to the primary signal and $1-\alpha$ fractional power to the secondary signal. Thereafter, the received signal at $\mathsf{PN_b}$ in the second phase is multiplied by $N_b \times 1$ receive beamforming weight vector $\widehat{\mathbf{w_b}}$ for maximum ratio combining and the resultant signal is thus expressed as

$$y_{t,b} = \widehat{\mathbf{w_b}}^T \boldsymbol{h}_{t,b}(x_a^{\text{II}} + \eta_{tbp}) + \widehat{\mathbf{w_b}}^T \boldsymbol{h}_{t,b}(x_s + \eta_{tbs}) + \widehat{\mathbf{w_b}}^T \boldsymbol{n_b}, \tag{9}$$

where x_a^{II} is the symbol transmitted from $\mathsf{SN_t}$ to $\mathsf{PN_b}$ in the second phase and x_s is the symbol transmitted from $\mathsf{SN_t}$ to $\mathsf{SN_r}$ with $\mathbb{E}\{|x_a^{\text{II}}|^2\} = \alpha P_h$ and $\mathbb{E}\{|x_s|^2\} = (1-\alpha)P_h$. $\eta_{tbp} \sim \mathcal{CN}(0, k^2\alpha P_h)$ and $\eta_{tbs} \sim \mathcal{CN}(0, k^2(1-\alpha)P_h)$ are the distortion noises caused due to HIs. The receive beamforming weight vector is given by $\widehat{\mathbf{w_b}}^T = \left(\frac{\boldsymbol{h}_{t,b}^\dagger}{\|\boldsymbol{h}_{t,b}\|}\right)$, $\boldsymbol{n_b}$ is the $N_b \times 1$ AWGN vector at node $\mathsf{PN_b}$, and $\widehat{\mathbf{w_b}}^T \boldsymbol{n_b} \sim \mathcal{CN}(0, \sigma_b^2)$. Based on (6) and (9), the SNDR at $\mathsf{PN_b}$ is given as

$$\gamma_{t,b} = \begin{cases} \gamma_{t,b}^{\text{lin}} & \text{for} \quad P_a\|\boldsymbol{h}_{a,t}\|^2 \leq P_{\text{th}} \\ \gamma_{t,b}^{\text{sat}} & \text{for} \quad P_a\|\boldsymbol{h}_{a,t}\|^2 > P_{\text{th}}, \end{cases} \tag{10}$$

where $\gamma_{t,b}^{\text{lin}}$ denotes the SNDR when the EH circuit is operating in linear region while $\gamma_{t,b}^{\text{sat}}$ represents the SNDR when it is in saturation region. $\gamma_{t,b}^{\text{lin}}$ and $\gamma_{t,b}^{\text{sat}}$ are given as follows

$$\gamma_{t,b}^{\text{lin}} = \frac{\alpha\beta\eta P_a \|\boldsymbol{h}_{a,t}\|^2 \|\boldsymbol{h}_{t,b}\|^2}{(1-\alpha+k^2)\beta\eta P_a \|\boldsymbol{h}_{a,t}\|^2 \|\boldsymbol{h}_{t,b}\|^2 + \sigma_b^2} \tag{11}$$

$$\gamma_{t,b}^{\text{sat}} = \frac{\alpha\beta\eta P_{\text{th}} \|\boldsymbol{h}_{t,b}\|^2}{(1-\alpha+k^2)\beta\eta P_{\text{th}} \|\boldsymbol{h}_{t,b}\|^2 + \sigma_b^2}. \tag{12}$$

The achievable rate at $\mathsf{PN_b}$ is $\mathcal{R}_{t,b} = \frac{1}{2}\log_2(1+\gamma_{t,b})$. During the second phase, the signal received at $\mathsf{SN_r}$ is given as

$$y_{t,r} = h_{t,r}(x_a^{\text{II}} + \eta_{trp}) + h_{t,r}(x_s + \eta_{trs}) + n_r, \tag{13}$$

where $h_{t,r}$ denotes the channel coefficient between $\mathsf{SN_t}$ and $\mathsf{SN_r}$, $\eta_{trp} \sim \mathcal{CN}(0, k^2\alpha P_h)$ and $\eta_{trs} \sim \mathcal{CN}(0, k^2(1-\alpha)P_h)$ are the distortion noises caused due to HIs corresponding to primary and secondary symbols respectively and $n_r \sim \mathcal{CN}(0, \sigma_r^2)$ represents the AWGN noise at $\mathsf{SN_r}$. After primary interference cancellation, the SNDR at $\mathsf{SN_r}$ is given as follows

$$\gamma_{t,r} = \frac{(1-\alpha)P_h|h_{t,r}|^2}{k^2 P_h |h_{t,r}|^2 + \sigma_r^2}. \tag{14}$$

Considering P_h from (6) in the above expression, we have

$$\gamma_{t,r} = \begin{cases} \gamma_{t,r}^{\text{lin}} & \text{for} \quad P_a\|\boldsymbol{h}_{a,t}\|^2 \le P_{\text{th}} \\ \gamma_{t,r}^{\text{sat}} & \text{for} \quad P_a\|\boldsymbol{h}_{a,t}\|^2 > P_{\text{th}}, \end{cases} \tag{15}$$

where $\gamma_{t,r}^{\text{lin}}$ and $\gamma_{t,r}^{\text{sat}}$ are expressed as

$$\gamma_{t,r}^{\text{lin}} = \frac{(1-\alpha)\beta\eta P_a \|\boldsymbol{h}_{a,t}\|^2 |h_{tr}|^2}{k^2\beta\eta P_a \|\boldsymbol{h}_{a,t}\|^2 |h_{t,r}|^2 + \sigma_r^2} \tag{16}$$

$$\gamma_{t,r}^{\text{sat}} = \frac{(1-\alpha)\beta\eta P_{\text{th}} |h_{t,r}|^2}{k^2\beta\eta P_{\text{th}} |h_{tr}|^2 + \sigma_r^2}. \tag{17}$$

The achievable rate in the second phase between $\mathsf{SN_t}$ and $\mathsf{SN_r}$ is given by $\mathcal{R}_{t,r} =$ $\frac{1}{2}\log_2(1+\gamma_{t,r})$.

3. Performance Analysis

3.1. OP for Primary Link

The primary link $\mathsf{PN_a}\rightarrow\mathsf{PN_b}$ will be in outage if the instantaneous achievable rate $\mathcal{R}_{a,t}$ at $\mathsf{SN_t}$ or the instantaneous achievable rate $\mathcal{R}_{t,b}$ at $\mathsf{PN_b}$ falls below a predefined target rate. Here, the term $\mathcal{R}_{t,b}$ may also depend on $\|\boldsymbol{h}_{a,t}\|^2$ along with $\mathcal{R}_{a,t}$, as the transmit power P_h in the second phase becomes a function of $\|\boldsymbol{h}_{a,t}\|^2$ in the linear region. However, taking into account the tractability of the subsequent mathematical analysis with a non-linear EH model, the OP for the primary link is formulated as in [19, 43, 44],

$$\mathcal{P}_{\text{out},b} = 1 - \Pr[\mathcal{R}_{a,t} \geq r_b]\Pr[\mathcal{R}_{t,b} \geq r_b]. \tag{18}$$

The above expression can be evaluated by solving individual probability terms. The term $\Pr[\mathcal{R}_{a,t} \geq r_b]$ is solved as follows.

$$\begin{aligned}\Pr[\mathcal{R}_{a,t} \geq r_b] &= 1 - \Pr[\mathcal{R}_{a,t} < r_b] = 1 - \Pr[\gamma_{a,t} < \varphi_b] \\ &\triangleq 1 - F_{\gamma_{a,t}}(\varphi_b),\end{aligned} \tag{19}$$

where $\varphi_b = 2^{2r_b} - 1$ is the desired target signal-to-noise ratio (SNR). The term $F_{\gamma_{a,t}}(\varphi_b)$ is formulated as

$$F_{\gamma_{a,t}}(\varphi_b) = \Pr\left[\|\boldsymbol{h}_{a,t}\|^2 < \frac{\varphi_b((1-\beta)\sigma_t^2 + \sigma_{cr}^2)}{(1-\beta)P_a(1-k^2\varphi_b)}\right]. \tag{20}$$

On incorporating the PDF expression of $\|\boldsymbol{h}_{a,t}\|^2$ in the above probability term and solving the resulting integral as shown in Appendix A, the expression of $F_{\gamma_{a,t}}(\varphi_b)$ can be obtained as

$$F_{\gamma_{a,t}}(\varphi_b) = \frac{1}{\Gamma[m_{at}N_a]}\Upsilon\left[m_{at}N_a, \frac{m_{at}}{\Omega_{at}}\frac{\varphi_b((1-\beta)\sigma_t^2+\sigma_{cr}^2)}{(1-\beta)P_a(1-k^2\varphi_b)}\right]. \tag{21}$$

On similar grounds as in (19), the second probability term in (18) can be expressed as

$$\Pr[\mathcal{R}_{t,b} \geq r_b] \triangleq 1 - F_{\gamma_{t,b}}(\varphi_b). \tag{22}$$

Further, $F_{\gamma_{t,b}}(\varphi_b)$ can be formulated as

$$F_{\gamma_{t,b}}(\varphi_b) = \Pr[\gamma_{t,b} < \varphi_b], \tag{23}$$

which can be then expressed for two cases as

$$\begin{aligned} F_{\gamma_{t,b}}(\varphi_b) = &\Pr[\gamma_{t,b}^{\text{lin}} < \varphi_b, P_a \|\boldsymbol{h}_{a,t}\|^2 \leq P_{\text{th}}] \\ &+ \Pr[\gamma_{t,b}^{\text{sat}} < \varphi_b, P_a \|\boldsymbol{h}_{a,t}\|^2 > P_{\text{th}}]. \end{aligned} \tag{24}$$

Therefore, (24) can be represented as

$$F_{\gamma_{t,b}}(\varphi_b) = F_{\gamma_{t,b}^{\text{lin}}}(\varphi_b) + F_{\gamma_{t,b}^{\text{sat}}}(\varphi_b). \tag{25}$$

Hereby, $F_{\gamma_{t,b}^{\text{lin}}}(\varphi_b)$ is obtained as follows.

$$\begin{aligned} F_{\gamma_{t,b}^{\text{lin}}}(\varphi_b) = &\frac{1}{\Gamma[m_{at}N_a]} \frac{1}{\Gamma[m_{tb}N_b]} \Upsilon\left[m_{at}N_a, \frac{m_{at}}{\Omega_{at}} \frac{P_{\text{th}}}{P_a}\right] \\ &\times \Upsilon\left[m_{tb}N_b, \frac{m_{tb}}{\Omega_{tb}} \frac{\epsilon_b}{P_{\text{th}}}\right] + \frac{\Gamma\left[m_{tb}N_b, \frac{m_{tb}}{\Omega_{tb}} \frac{\epsilon_b}{P_{\text{th}}}\right]}{\Gamma[m_{tb}N_b]} \\ &- \frac{1}{\Gamma[m_{tb}N_b]} \left(\frac{m_{tb}}{\Omega_{tb}}\right)^{m_{tb}N_b} \sum_{i=0}^{m_{at}N_a - 1} \frac{\left(\frac{m_{at}}{\Omega_{at}} \frac{\epsilon_b}{P_a}\right)^i}{i!} \\ &\times \left(2 \left(\frac{\frac{m_{at}}{\Omega_{at}} \frac{\epsilon_b}{P_a}}{\frac{m_{tb}}{\Omega_{tb}}} \right)^{\frac{m_{tb}N_b - i}{2}} \mathcal{K}_{m_{tb}N_b - i} \left(2 \sqrt{\frac{m_{at}}{\Omega_{at}} \frac{\epsilon_b}{P_a} \frac{m_{tb}}{\Omega_{tb}}} \right) \right. \\ &- \sum_{s=0}^{\infty} \frac{(-1)^s}{s!} \left(\frac{m_{tb}}{\Omega_{tb}}\right)^s \left(\frac{m_{at}}{\Omega_{at}} \frac{\epsilon_b}{P_a}\right)^{m_{tb}N_b - i + s} \\ &\times \left(\frac{m_{at}}{\Omega_{at}} \frac{P_{\text{th}}}{P_a}\right)^{-\frac{1}{2}(m_{tb}N_b - i + s + 1)} \mathrm{e}^{-\frac{1}{2}\left(\frac{m_{at}}{\Omega_{at}} \frac{P_{\text{th}}}{P_a}\right)} \\ &\left. \times \mathcal{W}_{-\frac{1}{2}(m_{tb}N_b - i + s + 1), -\frac{1}{2}(m_{tb}N_b - i + s)} \left[\frac{m_{at}}{\Omega_{at}} \frac{P_{\text{th}}}{P_a}\right] \right), \end{aligned} \tag{26}$$

and the expression of $F_{\gamma_{t,b}^{\text{sat}}}(\varphi_b)$ is given by

$$\begin{aligned} F_{\gamma_{t,b}^{\text{sat}}}(\varphi_b) = &\frac{1}{\Gamma[m_{at}N_a]} \frac{1}{\Gamma[m_{tb}N_b]} \Gamma\left[m_{at}N_a, \frac{m_{at}}{\Omega_{at}} \frac{P_{\text{th}}}{P_a}\right] \\ &\times \Upsilon\left[m_{tb}N_b, \frac{m_{tb}}{\Omega_{tb}} \frac{\epsilon_b}{P_{\text{th}}}\right], \end{aligned} \tag{27}$$

where $\epsilon_b = \frac{\sigma_b^2 \varphi_b}{\beta\eta(\alpha - (1-\alpha+k^2)\varphi_b)}$.

Proof: Please see Appendix A.

Thereafter, $F_{\gamma_{t,b}}(\varphi_b)$ is obtained by substituting (26) and (27) in (25). Moreover, based on (19) and (22), $\mathcal{P}_{\text{out},b}$ in (18) can be expressed as follows

$$\mathcal{P}_{\text{out},b} = 1 - (1 - F_{\gamma_{a,t}}(\varphi_b))(1 - F_{\gamma_{t,b}}(\varphi_b)). \tag{28}$$

Inserting the expressions obtained from (21) and (25) into (28), the exact expression for $\mathcal{P}_{\text{out},b}$ can readily be obtained.

3.2. OP for Secondary Link

The secondary link $\mathsf{SN_t}\rightarrow\mathsf{SN_r}$ will be in outage if the desired target rate at $\mathsf{SN_r}$ exceeds the instantaneous achievable rate $\mathcal{R}_{t,r}$ or if $\mathsf{SN_r}$ fails to decode the symbol x_a. Considering the decoding events to be independent, the OP at $\mathsf{SN_r}$ can be expressed as in [19, 43],

$$\mathcal{P}_{\text{out},r} = 1 - \Pr[\mathcal{R}_{a,t} \geq r_b]\Pr[\mathcal{R}_{t,r} \geq r_s]. \tag{29}$$

where r_s is the desired target rate at node $\mathsf{SN_r}$. In the above equation, the first probability term has already been solved in (19), while the second probability term is formulated as follows

$$\begin{aligned}\Pr[\mathcal{R}_{t,r} \geq r_s] &= 1 - \Pr[\mathcal{R}_{t,r} < r_s] = 1 - \Pr[\gamma_{t,r} < \varphi_s] \\ &\triangleq 1 - F_{\gamma_{t,r}}(\varphi_s),\end{aligned} \tag{30}$$

where $\varphi_s = 2^{2r_s} - 1$ is the pre-defined target SNR at secondary node $\mathsf{SN_r}$. Thus, from (19) and (30), $\mathcal{P}_{\text{out},r}$ in (29) can be given as

$$\mathcal{P}_{\text{out},r} = 1 - (1 - F_{\gamma_{a,t}}(\varphi_b))(1 - F_{\gamma_{t,r}}(\varphi_s)). \tag{31}$$

Further, $F_{\gamma_{t,r}}(\varphi_s)$ can be expressed as

$$\begin{aligned}F_{\gamma_{t,r}}(\varphi_s) = &\Pr[\gamma_{t,r}^{\text{lin}} < \varphi_s, P_a\|\boldsymbol{h}_{a,t}\|^2 \leq P_{\text{th}}] \\ &+ \Pr[\gamma_{t,r}^{\text{sat}} < \varphi_s, P_a\|\boldsymbol{h}_{a,t}\|^2 > P_{\text{th}}].\end{aligned} \tag{32}$$

Therefore, (32) can be represented as

$$F_{\gamma_{t,r}}(\varphi_s) = F_{\gamma_{t,r}^{\text{lin}}}(\varphi_s) + F_{\gamma_{t,r}^{\text{sat}}}(\varphi_s). \tag{33}$$

The exact expression of CDF $F_{\gamma_{t,r}^{\text{lin}}}(\varphi_s)$ is given as

$$
\begin{aligned}
F_{\gamma_{t,r}^{\text{lin}}}(\varphi_s) = & \frac{1}{\Gamma[m_{tr}]}\frac{1}{\Gamma[m_{at}N_a]}\Upsilon\left[m_{at}N_a, \frac{m_{at}}{\Omega_{at}}\frac{P_{\text{th}}}{P_a}\right] \\
& \times \Upsilon\left[m_{tr}, \frac{m_{tr}}{\Omega_{tr}}\frac{\epsilon_r}{P_{\text{th}}}\right] + \frac{\Gamma\left[m_{tr}, \frac{m_{tr}}{\Omega_{tr}}\frac{\epsilon_r}{P_{\text{th}}}\right]}{\Gamma[m_{tr}]} \\
& - \frac{1}{\Gamma[m_{tr}]}\left(\frac{m_{tr}}{\Omega_{tr}}\right)^{m_{tr}}{}^{m_{at}N_a-1} \sum_{i=0}^{} \frac{\left(\frac{m_{at}}{\Omega_{at}}\frac{\epsilon_r}{P_a}\right)^i}{i!} \\
& \times \left(2\left(\frac{\frac{m_{at}}{\Omega_{at}}\frac{\epsilon_r}{P_a}}{\frac{m_{tr}}{\Omega_{tr}}}\right)^{\frac{m_{tr}-i}{2}} \mathcal{K}_{m_{tr}-i}\left(2\sqrt{\frac{m_{at}}{\Omega_{at}}\frac{\epsilon_r}{P_a}\frac{m_{tr}}{\Omega_{tr}}}\right)\right. \\
& - \sum_{s=0}^{\infty}\frac{(-1)^s}{s!}\left(\frac{m_{tr}}{\Omega_{tr}}\right)^s\left(\frac{m_{at}}{\Omega_{at}}\frac{\epsilon_r}{P_a}\right)^{m_{tr}-i+s} \\
& \times \left(\frac{m_{at}}{\Omega_{at}}\frac{P_{\text{th}}}{P_a}\right)^{-\frac{1}{2}(m_{tr}-i+s+1)} \text{e}^{-\frac{1}{2}\left(\frac{m_{at}}{\Omega_{at}}\frac{P_{\text{th}}}{P_a}\right)} \\
& \left. \times \mathcal{W}_{-\frac{1}{2}(m_{tr}-i+s+1),-\frac{1}{2}(m_{tr}-i+s)}\left[\frac{m_{at}}{\Omega_{at}}\frac{P_{\text{th}}}{P_a}\right]\right). \qquad (34)
\end{aligned}
$$

Equation (34) is valid for the condition $1-\alpha-k^2r_s > 0$, else $F_{\gamma_{t,r}^{\text{lin}}}(\varphi_s) = 1$. Moreover, the term $F_{\gamma_{t,r}^{\text{sat}}}(\varphi_s)$ can be obtained as

$$
\begin{aligned}
F_{\gamma_{t,r}^{\text{sat}}}(\varphi_s) = & \frac{1}{\Gamma[m_{at}N_a]}\frac{1}{\Gamma[m_{tr}]}\Gamma\left[m_{at}N_a, \frac{m_{at}}{\Omega_{at}}\frac{P_{\text{th}}}{P_a}\right] \\
& \times \Upsilon\left[m_{tr}, \frac{m_{tr}}{\Omega_{tr}}\frac{\epsilon_r}{P_{\text{th}}}\right]. \qquad (35)
\end{aligned}
$$

where $\epsilon_r = \frac{r_s\sigma_r^2}{\beta\eta(1-\alpha-k^2r_s)}$.

Proof: Please see Appendix B.

Hence, $F_{\gamma_{t,r}}(\varphi_s)$ is obtained by incorporating the expressions in (34) and (35) in (33). The final exact expression of $\mathcal{P}_{\text{out},r}$ is obtained by substituting (21) and (33) in (31).

Remarks: The expressions of $\mathcal{P}_{\text{out},b}$ and $\mathcal{P}_{\text{out},r}$ can be validated for special cases as given below.

Case 1: On assuming ideal hardware circuitry at all the nodes, i.e., $k^2 = 0$, with the consideration of $N_a = N_b = 1$ and a linear EH model SWIPT receiver

at the secondary node, these expressions converge to those given in [43].

Case 2: When the impact of HIs at all the communicating nodes is taken into account with a single antenna source and the linear EH enabled receiver at $\mathsf{SN_t}$, the derived OP expressions for both primary and secondary nodes reduce to the expressions as derived in [45].

3.3. System Throughput

In a communication system under delay-limited transmission scenario, system throughput is the total average target rates of both primary and secondary nodes attained over fading channels. Therefore, system throughput $\mathbb{S}_T$ for the considered scheme can be expressed as [41]

$$\mathbb{S}_T = \frac{1}{2}\big(r_b\left(1-\mathcal{P}_{\text{out},b}\right) + r_s\left(1-\mathcal{P}_{\text{out},r}\right)\big), \tag{36}$$

where $\mathcal{P}_{\text{out},b}$ and $\mathcal{P}_{\text{out},r}$ are obtained in (28) and (31), respectively.

3.4. Asymptotic Analysis

To obtain significant insights into the performance of the considered system with HIs and multiple antenna sources, asymptotic outage behavior is analyzed in the high SNR regime. Performing some mathematical manipulations and approximating $\Upsilon[x,z] \underset{z\to 0}{\approx} \frac{z^x}{x}$ [46] in solving the integrals forms given in (A.1), (A.3) and (A.5), the asymptotic outage probability at primary node $\mathsf{PN_b}$, is expressed as

$$\begin{aligned}\mathcal{P}_{\text{out},b}^{\text{asym}} = \frac{1}{\Gamma[m_{at}N_a]\Gamma[m_{tb}N_b]}\Bigg(&\frac{1}{m_{at}N_a}\left(\frac{m_{at}}{\Omega_{at}}\right)^{m_{at}N_a}\\
&\times\Bigg(\Upsilon\left[m_{tb}N_b, \frac{m_{tb}\epsilon_b}{\Omega_{tb}P_{\text{th}}}\right]\left(\frac{P_{\text{th}}}{P_a}\right)^{m_{at}N_a} + \left(\frac{m_{tb}}{\Omega_{tb}}\right)^{m_{at}N_a}\\
&\times\left(\frac{\epsilon_b}{P_a}\right)^{m_{at}N_a}\Gamma\left[m_{tb}N_b - m_{at}N_a, \frac{m_{tb}\epsilon_b}{\Omega_{tb}P_{\text{th}}}\right]\Bigg)\\
&+\Upsilon\left[m_{tb}N_b, \frac{m_{tb}\epsilon_b}{\Omega_{tb}P_{\text{th}}}\right]\Bigg(\Gamma[m_{at}N_a] - \frac{1}{m_{at}N_a}\\
&\times\left(\frac{m_{at}}{\Omega_{at}}\frac{P_{\text{th}}}{P_a}\right)^{m_{at}N_a}\Bigg)\Bigg).\end{aligned} \tag{37}$$

Similarly, the asymptotic outage probability at secondary node $\mathsf{SN_r}$, is given as

$$\begin{aligned}\mathcal{P}_{\mathrm{out},r}^{\mathrm{asym}} = \frac{1}{\Gamma[m_{at}N_a]\Gamma[m_{tr}]}\Bigg(\frac{1}{m_{at}N_a}\left(\frac{m_{at}}{\Omega_{at}}\right)^{m_{at}N_a} \\ \times\Bigg(\Upsilon\left[m_{tr},\frac{m_{tr}\epsilon_r}{\Omega_{tr}P_{\mathrm{th}}}\right]\left(\frac{P_{\mathrm{th}}}{P_a}\right)^{m_{at}N_a}+\left(\frac{m_{tr}}{\Omega_{tr}}\right)^{m_{at}N_a} \\ \times\left(\frac{\epsilon_r}{P_a}\right)^{m_{at}N_a}\Gamma\left[m_{tr}-m_{at}N_a,\frac{m_{tr}\epsilon_r}{\Omega_{tr}P_{\mathrm{th}}}\right]\Bigg) \\ +\Upsilon\left[m_{tr},\frac{m_{tr}\epsilon_r}{\Omega_{tr}P_{\mathrm{th}}}\right]\Bigg(\Gamma[m_{at}N_a]-\frac{1}{m_{at}N_a} \\ \times\left(\frac{m_{at}}{\Omega_{at}}\frac{P_{\mathrm{th}}}{P_a}\right)^{m_{at}N_a}\Bigg)\Bigg). \end{aligned} \tag{38}$$

3.5. Optimization

In this section, we formulate and investigate two optimization problems, viz., 1) outage probability minimization at primary node, and 2) system throughput maximization. Under these two problems, we seek to obtain the optimal values of PS factor (β) and spectrum sharing factor (α) in what follows.

1) Problem formulation for primary outage probability minimization:

Here, the objective is to obtain optimal PS and spectrum sharing factors corresponding to minimum OP at $\mathsf{PN_b}$. As the asymptotic OP expression is found tight (demonstrated in Section 4), it can be considered to investigate the optimization problem of OP minimization at primary node.

Therefore, we can formulate the primary OP minimization problem as

$$\begin{aligned}\mathbf{P1}: \quad & \underset{\alpha,\beta}{\text{minimize}}\ \mathcal{P}_{\mathrm{out},b}^{\mathrm{asym}} \\ \text{s.t.} \quad & \text{(Power splitting constraint):} \\ & \mathrm{C}_1:\ 0<\beta<1 \\ & \text{(Spectrum sharing constraint):} \\ & \mathrm{C}_2:\ \alpha^*<\alpha<1\end{aligned} \tag{39}$$

where α^* is the critical value of α above which the relayed link outperforms the direct link. α^* varies with the considered set of system parameters and is

obtained as shown in Fig. 7 in Section 4. The outage probability of primary link is convex as its Hessian is found to be positive definite as given in Appendix C, and thus the corresponding unconstrained minimization problem can be solved from the zero-gradient conditions [47] i.e., $\frac{\partial \mathcal{P}_{\text{out},b}^{\text{asym}}}{\partial \alpha} = 0$ and $\frac{\partial \mathcal{P}_{\text{out},b}^{\text{asym}}}{\partial \beta} = 0$, where $\frac{\partial P_{out,b}^{asym}}{\partial \alpha}$ and $\frac{\partial P_{out,b}^{asym}}{\partial \beta}$ are given in (C.1) and (C.2), respectively.

2) Problem formulation for maximizing system throughput:

Here, we strive to maximize the system throughput and thereby find the corresponding optimal PS and spectrum sharing factors while maintaining the QoS for the primary link. The maximization problem is formulated as follows.

$$\begin{aligned} \mathbf{P2}: \quad & \underset{\alpha,\beta}{\text{maximize}}\ \mathbb{S}_T \\ \text{s.t.} \quad & \text{(Power splitting constraint):} \\ & \mathrm{C}_1: \ 0 < \beta < 1 \\ & \text{(Spectrum sharing constraint):} \\ & \mathrm{C}_2: \ \alpha^* < \alpha < 1 \\ & \text{(QoS constraint):} \\ & \mathrm{C}_3: \ \mathcal{P}_{\text{out},b} \leq \mathcal{P}_{\text{out},b}^{max} \end{aligned} \tag{40}$$

Here, $\mathcal{P}_{\text{out},b}^{max}$ is the maximum permissible outage probability at the primary node to ensure QoS at the primary nodes. The above non-linear programming problem is a constrained optimization wherein constraint C_3 is a convex function. Hence, it is solved using KKT conditions [44]. To proceed further, we first define the Lagrangian function for the above maximization problem as

$$\begin{aligned} \mathbb{L}\left(\beta, \alpha : \lambda_1, \lambda_2, \lambda_3\right) = \mathbb{S}_T + \lambda_1 \left(1 - \beta\right) + \lambda_2 \left(1 - \alpha\right) \\ + \lambda_3 \left(\mathcal{P}_{\text{out},b}^{max} - \mathcal{P}_{\text{out},b}\right), \end{aligned} \tag{41}$$

where λ_1, λ_2 and λ_3 are the Lagrangian multipliers for the problem constraints $\mathrm{C}_1, \mathrm{C}_2$ and C_3 respectively. Thus, the optimal condition is given as,

$$\nabla \mathbb{L}\left(\beta, \alpha : \lambda_1, \lambda_2, \lambda_3\right) = 0. \tag{42}$$

The complementary slackness conditions are expressed as

$$\lambda_1 (1 - \beta) = 0, \tag{43}$$

$$\lambda_2 (1 - \alpha) = 0, \tag{44}$$

$$\lambda_3 \left(\mathcal{P}_{\text{out},b}^{max} - \mathcal{P}_{\text{out},b} \right) = 0. \tag{45}$$

The non-negativity conditions of the Lagrangian multipliers based on the constraints is given as $\lambda_1 \geq 0, \lambda_2 \geq 0$ and $\lambda_3 \geq 0$. Adhering to the above mentioned conditions and solving the equations, for a given set of system parameters, we can obtain the optimal PS and spectrum sharing factors corresponding to maximum throughput. It is apparent from the complementary slackness conditions that when $\lambda_1, \lambda_2 \neq 0$, it results in $\beta = \alpha = 1$, which is not a feasible solution for the considered system model and hence $\lambda_1, \lambda_2 = 0$. When $\lambda_3 \neq 0$, solving the equations obtained from (42) and (45), the feasible solution is obtained for the maximization problem where λ_3 satisfies the non-negativity condition.

4. Results and Discussion

A 2-D network topology is considered wherein the primary nodes $\mathsf{PN_a}$ and $\mathsf{PN_b}$ are placed at coordinates (0,0) and (4,0) respectively, while the secondary nodes $\mathsf{SN_t}$ and $\mathsf{SN_r}$ are assumed to be at (2,0) and (2,2) respectively. A path loss model with path loss exponent $\nu = 3$ is adopted and hence the variances of channel gains are defined as $\Omega_{ij} = d_{ij}^{-\nu}$, where d_{ij} is the distance between two nodes i and j. Moreover, it is assumed that $\sigma_b^2 = \sigma_t^2 = \sigma_r^2 = \sigma_{rf}^2 = \sigma^2$ and the transmit SNR is defined as P_a/σ^2. The threshold power of the non-linear EH circuit P_{th} is set as -10dBm, noise power at the primary and secondary nodes is considered to be -40dBm and $\eta = 0.7$. Further, $N_a = N_b = 2$ unless otherwise mentioned in the figure. The remaining parameters which vary with each figure are defined therein. As depicted in Table 1, for the considered set of system design parameters, the infinite series involved in (28) and (31) are truncated to include the first 15 terms for achieving sufficient accuracy (up to first seven decimal places) in all the analytical results.

Table 1: Number of terms required in infinite series of (28) and (31) for achieving accuracy up to first seven decimal places.

Index s	$P_{\text{out},b}$ in (28)		$P_{\text{out},r}$ in (31)	
	SNR = 21dB	23dB	20dB	25dB
1	0.446043	0.216307	0.940947	0.422053
2	0.446048	0.216542	0.940972	0.581568
3	0.446046	0.216436	0.940958	0.494169
4	0.446047	0.216472	0.940964	0.530428
5	0.446047	0.216462	0.940962	0.518296
6	0.446047	0.216465	0.940963	0.521702
7	0.446047	0.216464	0.940962	0.520877
8	0.446047	0.216464	0.940962	0.521053
9	0.446047	0.216464	0.940962	0.52102
10	0.446047	0.216464	0.940962	0.521025
11	0.446047	0.216464	0.940962	0.521025
12	0.446047	0.216464	0.940962	0.521025
13	0.446047	0.216464	0.940962	0.521025
14	0.446047	0.216464	0.940962	0.521025
15	0.446047	0.216464	0.940962	0.521025

Table 2: Optimal design parameters corresponding to maximum system throughput.

Target rate	SNR = 25dB		SNR = 30dB	
	α	β	α	β
1/2	0.7	0.58	0.899	0.899
1/3	0.6	0.5	0.7	0.9
1/4	0.49	0.9	0.43	0.81
1/5	0.31	0.9	0.4	0.9

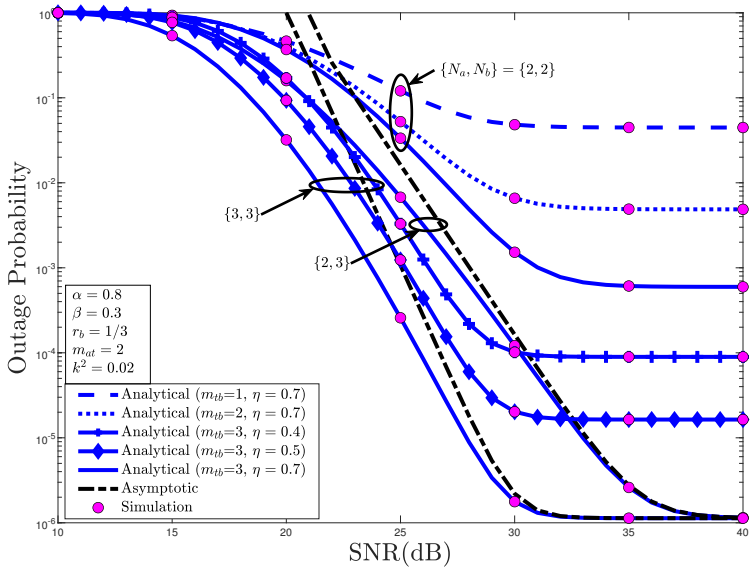

Figure 3: OP versus SNR for primary link.

Fig. 3 illustrates the OP for primary link with varying SNR for different fading scenarios and transmit and receive antennas. It can be observed that the outage performance improves with increasing fading severity parameter due to the fact that the link reliability is better in a less fading environment. Also, increase in the number of transmit/receive antennas causes better transmission reliability and hence it improves the outage performance. While the OP decreases with increasing transmit SNR, it remains saturated after a certain point which is attributed to the non-linearity of the considered EH model. Moreover, increased transmit SNR results in low probability of outage occurrence and hence the outage performance is better in high SNR range. With better energy conversion efficiency η, the energy harvested at the secondary node increases. Accordingly, the primary signal can be broadcasted with increased power, resulting in improved outage performance at the primary node.

Fig. 4 represents the OP curves for primary link with varying target rate for different HI levels. We can observe that the outage performance degrades with increasing HI levels (denoted by k^2) because HIs contribute to increased

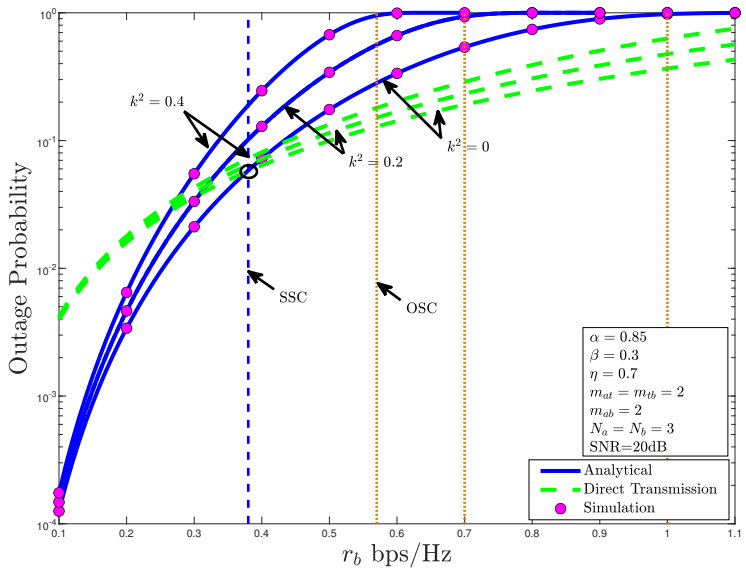

Figure 4: OP versus r_b for primary link.

distortion noise thereby increasing the OP. Also, two important phenomena, i.e., system spectrum ceiling (SSC) and overall system ceiling (OSC), are observed in this figure. Specifically, SSC gives the maximum achievable rate above which the system OP exceeds the OP of direct transmission link (if it exists). Hence for better primary link outage performance, the system has to be operated for target rates below SSC. Whereas, OSC is defined as the maximum attainable target rate above which the primary system goes into outage. Therefore, based on OSC it can be ensured that the primary link is not in outage. For the considered set of parameters as given in the figure and for $k^2 = 0.2$, the primary link is not in the outage for $r_b < 0.7$ bps/Hz. Moreover, to achieve better outage performance at the primary node than that of the direct link (if it exists), the target rate r_b should be below 0.32 bps/Hz.

Fig. 5 shows the OP for secondary link with varying α for different k and fading scenarios. It can be seen from this figure that increasing fading severity parameter improves the OP performance due to better link reliability, while increasing k^2 results in poor OP performance due to increased distortion noise.

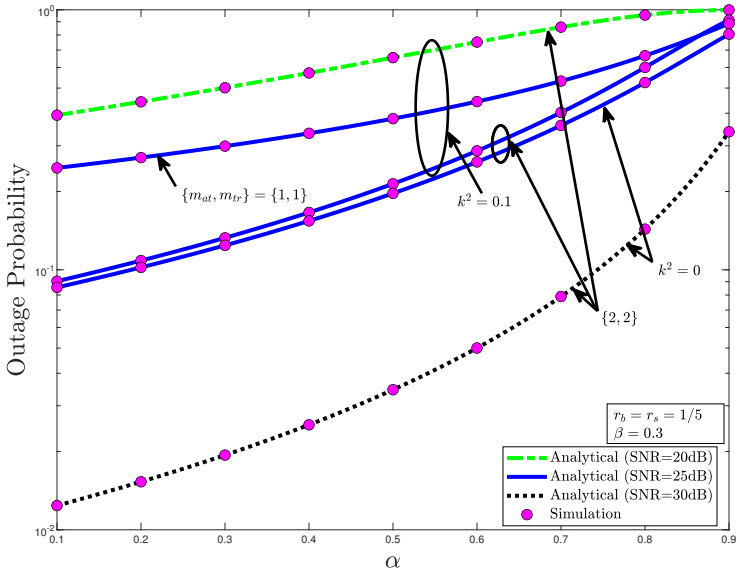

Figure 5: OP versus spectrum sharing factor for secondary link.

Also, OP is improved with increasing transmit SNR. Furthermore, the spectrum sharing factor α shows a significant impact on the OP of secondary node. For higher values of α, the OP increases drastically due to higher fraction of power being allotted for primary transmission while less amount of power is allocated for secondary transmission.

Fig. 6 describes the outage performance of the primary link with varying PS factor and SS factor. This plot shows the convex behavior of OP, which is in accordance with the mathematical analysis. It is to be noted that minimum OP is obtained for the given set of input parameters when $\alpha = 0.75$ and $\beta = 0.27$. Apparently, from the considered range of α, the obtained optimal value of α is relatively high. This attributes to the fact that when higher power is allotted for the primary signal transmission at the secondary node, the OP performance at the primary node is improved. Also, a lower β value implies that the major portion of the primary signal is used for information transmission rather than EH, which accounts for the minimal OP.

Fig. 7 discloses the behavior of outage performance of the primary link

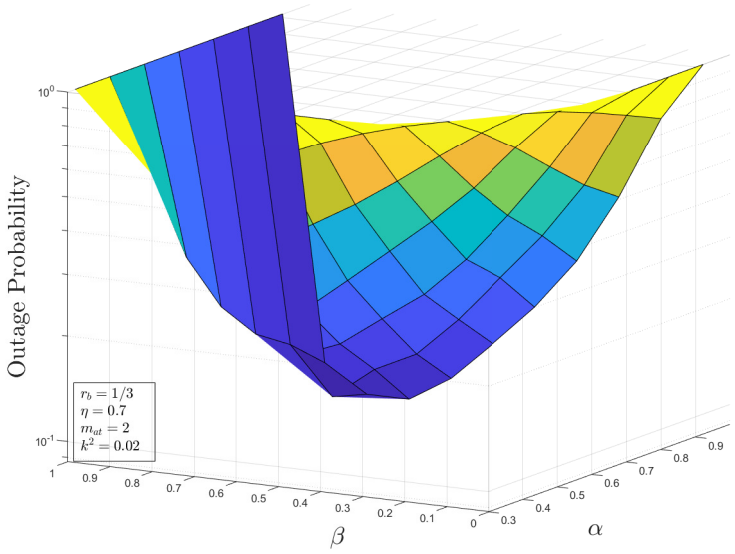

Figure 6: OP versus SNR for primary link.

versus spectrum sharing factor α for different target rates. OP of the direct transmission link is also plotted in this figure. From this plot, we can obtain the value of the spectrum sharing factor above which the relayed link performs better compared to the direct link. This value of α, i.e., α^* is called as critical value which plays a key role in ensuring effective spectrum sharing. Also, α^* increases with the target rate because an increase in the target rate needs higher transmit SNR. Thus, the power allocated for the primary signal transmission (determined by α) will increase.

Fig. 8 shows the system throughput curves with varying PS factor β, for different transmit SNR values and target rates. It is evident that in a particular SNR range, the system throughput is high and consistent. In order to obtain a significant throughput performance, the system has to be operated in a certain range of β, so that the OP at primary and secondary nodes together contribute to maximum system throughput. The feasible range of β lies between 0.7 to 0.9 corresponding to the considered target rate and transmit SNR.

Fig. 9 discloses the behavior of system throughput with varying α and β

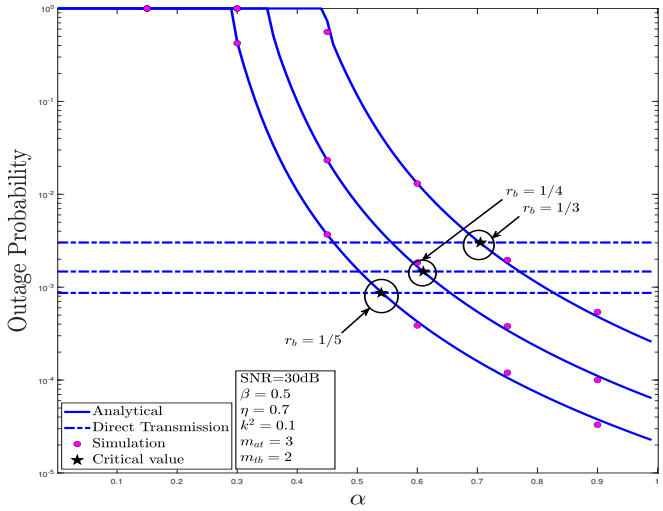

Figure 7: OP versus α for primary link.

values. It is evident from the plot that the system throughput variation for a given set of system parameters is loosely concave. Maximum system throughput can be achieved by considering a particular set of of α and β values, which are obtained by solving the optimization problem **P2**. Here, $\mathcal{P}_{\text{out},b}^{max}$ is assumed to be 0.005. The corresponding optimal values obtained for different target rates and transmit SNR are given in Table 2. It is observed that, as the target rate increases, the SS factor also increases in order to allot more power to the primary signal.

5. Conclusion

In this paper, we investigated the impact of hardware impairments on SWIPT-based CRN with multiple antennas at PNs. First, we proficiently obtained the outage probability expressions of both primary and secondary systems under the Nakagami-m fading environment. Further, the system throughput is also analyzed with the help of the derived OP expressions. Closed-form asymptotic expressions for primary and secondary OP in the high SNR regime are obtained to analyze the system performance. Two optimization problems, minimization

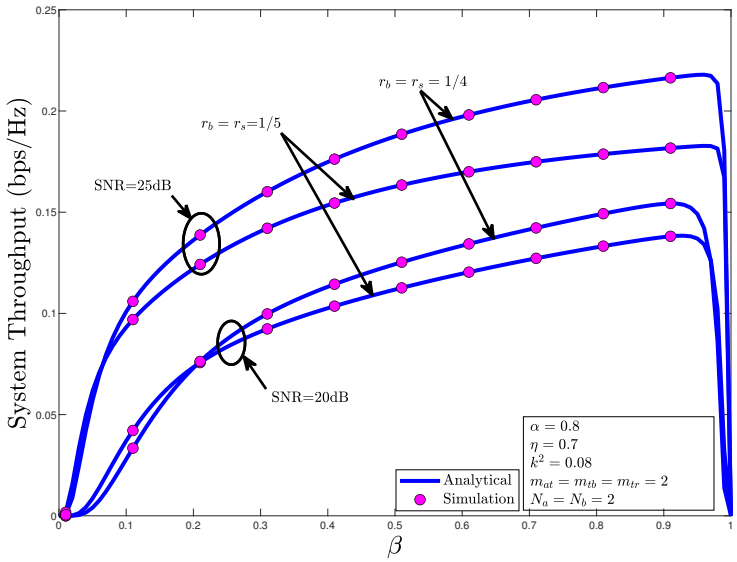

Figure 8: System throughput versus PS factor.

of OP and maximization of throughput, are formulated and their convexity is proved. The optimal PS and spectrum sharing factors are hence determined using KKT analysis. SSC and OSC effects are studied to give meaningful insights into the system behavior. It is observed that the hardware impairments degrade the system performance, which is countered using multiple antenna sources and designing the system with the achieved optimal parameters. The impact of various system and channel parameters on the system performance is studied comprehensively. Lastly, the analytical and simulation results validate the accuracy of the derived expressions.

CRediT authorship contribution statement

Addanki Prathima: Methodology, Investigation, Formal analysis, Writing - original draft, Data curation. **Devendra S. Gurjar**: Conceptualization, Methodology, Data curation, Supervision, Writing - reviewing and editing. **Yuming Jiang**: Writing - reviewing and editing, Supervision. **Suneel Yadav**: Writing - reviewing and editing, Supervision.

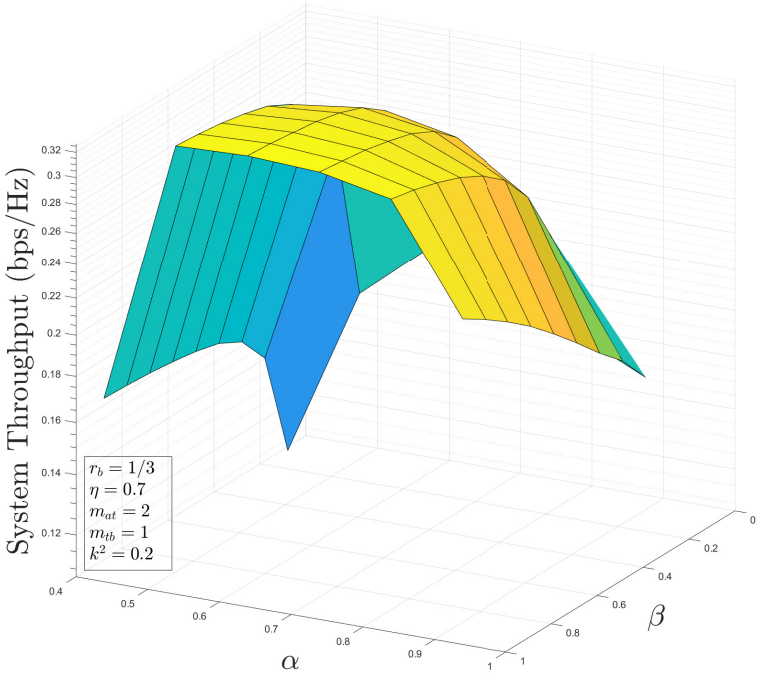

Figure 9: System throughput versus α and β.

Declaration of competing interest

The authors declare that they have no known competing financial interests or personal relationships that could have appeared to influence the work reported in this paper.

Appendix A.

Let $X = \|\boldsymbol{h}_{a,t}\|^2$ and $Y = \|\boldsymbol{h}_{t,b}\|^2$ be the Gamma distributed random variables whose PDFs are defined as [41] $f_X(x) = \left(\frac{m_{at}}{\Omega_{at}}\right)^{m_{at}N_a} \frac{x^{m_{at}N_a-1}}{\Gamma[m_{at}N_a]} \mathrm{e}^{-\frac{m_{at}}{\Omega_{at}}x}$, $x \geq 0$ and $f_Y(y) = \left(\frac{m_{tb}}{\Omega_{tb}}\right)^{m_{tb}N_b} \frac{y^{m_{tb}N_b-1}}{\Gamma[m_{tb}N_b]} \mathrm{e}^{-\frac{m_{tb}}{\Omega_{tb}}y}$, $y \geq 0$, respectively. The term $F_{\gamma_{a,t}}(\varphi_b)$ is formulated as,

$$F_{\gamma_{a,t}}(\varphi_b) = \Pr\left[X < \frac{\varphi_b((1-\beta)\sigma_t^2 + \sigma_{cr}^2)}{(1-\beta)P_a(1-k^2\varphi_b)}\right]. \tag{A.1}$$

Using [39, eq.(3.351.2)], the above expression can be expressed as in equation (21).

Furthermore, the CDF of $F_{\gamma_{t,b}^{\text{lin}}}(\varphi_b)$ can be formulated using (11) as,

$$\begin{aligned} F_{\gamma_{t,b}^{\text{lin}}}(\varphi_b) &= \Pr\left[\frac{\alpha\beta\eta P_a XY}{(1-\alpha+k^2)\beta\eta P_a XY+\sigma_b^2} < \varphi_b, P_a X \leq P_{\text{th}}\right], \\ &= \Pr\left[X < \frac{\epsilon_b}{P_a}\frac{1}{Y}, X \leq \frac{P_{\text{th}}}{P_a}\right], \end{aligned} \tag{A.2}$$

where $\epsilon_b = \frac{\sigma_b^2\varphi_b}{\beta\eta(\alpha-(1-\alpha+k^2)\varphi_b)}$. Hence, $F_{\gamma_{t,b}^{\text{lin}}}(\varphi_b)$ is expressed in integral form as follows.

$$\begin{aligned} F_{\gamma_{t,b}^{\text{lin}}}(\varphi_b) = &\int_{y=0}^{\frac{\epsilon_b}{P_{\text{th}}}} f_Y(y)dy \int_{x=0}^{\frac{P_{\text{th}}}{P_a}} f_X(x)dx \\ &+ \int_{y=\frac{\epsilon_b}{P_{\text{th}}}}^{\infty} f_Y(y)dy \int_{x=0}^{\frac{\epsilon_b}{P_a}\frac{1}{y}} f_X(x)dx. \end{aligned} \tag{A.3}$$

Applying the necessary mathematical manipulations as in [39, eqs. (3.381.6) and (3.471.9)], the above integral is solved as in (26). The CDF of $F_{\gamma_{t,b}^{\text{sat}}}(\varphi_b)$ is given as,

$$\begin{aligned} F_{\gamma_{t,b}^{\text{sat}}}(\varphi_b) &= \Pr\left[\frac{\alpha\beta\eta P_{\text{th}} Y}{(1-\alpha+k^2)\beta\eta P_{\text{th}} Y+\sigma_b^2} < \varphi_b, P_a X > P_{\text{th}}\right], \\ &= \Pr\left[Y < \frac{\epsilon_b}{P_{\text{th}}}, X > \frac{P_{\text{th}}}{P_a}\right]. \end{aligned} \tag{A.4}$$

The above probability expression is formulated in integral form as follows.

$$F_{\gamma_{t,b}^{\text{sat}}}(\varphi_b) = \int_{x=\frac{P_{\text{th}}}{P_a}}^{\infty} f_X(x)dx \int_{y=0}^{\frac{\epsilon_b}{P_{\text{th}}}} f_Y(y)dy. \tag{A.5}$$

Using [39, eqs. (3.351.1) and (3.351.2)], the above integral is solved as given in (27).

Appendix B.

Assuming, $Z = |h_{t,r}|^2$ is a Gamma distributed random variable with PDF $f_Z(z) = \left(\frac{m_{tr}}{\Omega_{tr}}\right)^{m_{tr}} \frac{z^{m_{tr}-1}}{\Gamma[m_{tr}]}\mathrm{e}^{-\frac{m_{tr}}{\Omega_{tr}}z}$, $z \geq 0$, the CDF of $F_{\gamma_{t,r}^{\text{lin}}}(\varphi_s)$ using (16) is

formulated as

$$F_{\gamma_{t,r}^{\text{lin}}}(\varphi_s) = \Pr\left[XZ < \frac{\epsilon_r}{P_a}, P_a X \leq P_{\text{th}}\right], \\ = \Pr\left[X < \frac{\epsilon_r}{P_a}\frac{1}{Z}, X \leq \frac{P_{\text{th}}}{P_a}\right], \tag{B.1}$$

where ϵ_r is defined after (35). This probability expression is formulated in integral form as

$$F_{\gamma_{t,r}^{\text{lin}}}(\varphi_s) = \int_{z=0}^{\frac{\epsilon_r}{P_{\text{th}}}} f_Z(z)dz \int_{x=0}^{\frac{P_{\text{th}}}{P_a}} f_X(x)dx \\ + \int_{z=\frac{\epsilon_r}{P_{\text{th}}}}^{\infty} f_Z(z)dz \int_{x=0}^{\frac{\epsilon_r}{P_a}\frac{1}{z}} f_X(x)dx. \tag{B.2}$$

The above integral is solved similar to (A.3) to obtain $F_{\gamma_{t,r}^{\text{lin}}}(\varphi_s)$ as given in (34). Using (17), the CDF of $F_{\gamma_{t,r}^{\text{sat}}}(\varphi_s)$ is given as

$$F_{\gamma_{t,r}^{\text{sat}}}(\varphi_s) = \Pr\left[\frac{(1-\alpha)\beta\eta P_{\text{th}} Z}{k^2\beta\eta P_{\text{th}} Z + \sigma_r^2} < \varphi_s, P_a X > P_{\text{th}}\right], \\ = \Pr\left[Z < \frac{\epsilon_r}{P_{\text{th}}}, X > \frac{P_{\text{th}}}{P_a}\right]. \tag{B.3}$$

The corresponding integral form is expressed as

$$F_{\gamma_{t,r}^{\text{sat}}}(\varphi_s) = \int_{x=\frac{P_{\text{th}}}{P_a}}^{\infty} f_X(x)dx \int_{z=0}^{\frac{\epsilon_r}{P_{\text{th}}}} f_Z(z)dz. \tag{B.4}$$

On similar grounds as in (A.5), the above integral is formulated as in (35).

Appendix C. Convexity of Objective Function

From the expression in (37), we obtain the expressions for the first derivative of $\mathcal{P}_{\text{out},b}^{\text{asym}}$ with respect to the two variables α and β as

$$\begin{aligned}\frac{\partial \mathcal{P}_{\text{out},b}^{\text{asym}}}{\partial \alpha} = & -\frac{1}{\Gamma[m_{at}N_a]\Gamma[m_{tb}N_b]}\frac{\varphi_b+1}{(\alpha-\varphi_b\,(1-\alpha+k^2))} \\ & \times \mathrm{e}^{-\frac{m_{tb}}{\Omega_{tb}}\frac{\epsilon_b}{P_{\text{th}}}}\left(\frac{m_{tb}}{\Omega_{tb}}\frac{\epsilon_b}{P_{\text{th}}}\right)^{m_{tb}N_b} + \frac{1}{\Gamma[m_{at}N_a+1]\Gamma[m_{tb}N_b]} \\ & \times \left(\frac{m_{at}}{\Omega_{at}}\right)^{m_{at}N_a}\left(-(\varphi_b+1)\frac{1}{(\alpha-\varphi_b\,(1-\alpha+k^2))}\right. \\ & \times \left(\frac{P_{\text{th}}}{P_a}\right)^{m_{at}N_a}\mathrm{e}^{-\frac{m_{tb}}{\Omega_{tb}}\frac{\epsilon_b}{P_{\text{th}}}}\left(\frac{m_{tb}}{\Omega_{tb}}\frac{\epsilon_b}{P_{\text{th}}}\right)^{m_{tb}N_b} \\ & + \mathrm{e}^{-\frac{m_{tb}}{\Omega_{tb}}\frac{\epsilon_b}{P_{\text{th}}}}(\varphi_b+1)\left(\frac{m_{tb}}{\Omega_{tb}}\right)^{m_{tb}N_b}\left(\frac{\epsilon_b}{P_a}\right)^{m_{at}N_a} \\ & \times \left(\frac{\epsilon_b}{P_{\text{th}}}\right)^{m_{tb}N_b-m_{at}N_a} - \frac{\varphi_b+1}{(\alpha-\varphi_b\,(1-\alpha+k^2))} \\ & \times m_{at}N_a\left(\frac{m_{tb}}{\Omega_{tb}}\right)^{m_{at}N_a}\left(\frac{\epsilon_b}{P_a}\right)^{m_{at}N_a} \\ & \left.\times\ \Gamma\left[m_{tb}N_b-m_{at}N_a,\frac{m_{tb}}{\Omega_{tb}}\frac{\epsilon_b}{P_{\text{th}}}\right]\right). \end{aligned} \tag{C.1}$$

$$\begin{aligned}\frac{\partial \mathcal{P}_{\text{out},b}^{\text{asym}}}{\partial \beta} = & -\frac{1}{\Gamma[m_{at}N_a]\Gamma[m_{tb}N_b]}\frac{1}{\beta}\left(\mathrm{e}^{-\frac{m_{tb}}{\Omega_{tb}}\frac{\epsilon_b}{P_{\text{th}}}}\left(\frac{m_{tb}}{\Omega_{tb}}\frac{\epsilon_b}{P_{\text{th}}}\right)^{m_{tb}N_b}\right. \\ & + \frac{1}{m_{at}N_a}\left(\frac{m_{at}}{\Omega_{at}}\right)^{m_{at}N_a}\left(-\mathrm{e}^{-\frac{m_{tb}}{\Omega_{tb}}\frac{\epsilon_b}{P_{\text{th}}}}\left(\frac{P_{\text{th}}}{P_a}\right)^{m_{at}N_a}\right. \\ & \times \left(\frac{m_{tb}}{\Omega_{tb}}\frac{\epsilon_b}{P_{\text{th}}}\right)^{m_{tb}N_b} + \mathrm{e}^{-\frac{m_{tb}}{\Omega_{tb}}\frac{\epsilon_b}{P_{\text{th}}}}\left(\frac{m_{tb}}{\Omega_{tb}}\right)^{m_{tb}N_b} \\ & \times \left(\frac{\epsilon_b}{P_a}\right)^{m_{at}N_a}\left(\frac{\epsilon_b}{P_{\text{th}}}\right)^{m_{tb}N_b-m_{at}N_a} \\ & - m_{at}N_a\left(\frac{m_{tb}}{\Omega_{tb}}\right)^{m_{at}N_a}\left(\frac{\epsilon_b}{P_a}\right)^{m_{at}N_a} \\ & \left.\left.\times\ \Gamma\left[m_{tb}N_b-m_{at}N_a,\frac{m_{tb}}{\Omega_{tb}}\frac{\epsilon_b}{P_{\text{th}}}\right]\right)\right). \end{aligned} \tag{C.2}$$

From the above two expressions, the second derivatives of $\mathcal{P}_{\text{out},b}^{\text{asym}}$ for the Hessian matrix are obtained as given in equations (C.3), (C.4) and (C.5). For the

considered range of input variables α and β, the Hessian matrix is found to be positive definite thus proving **P1** to be a convex optimization problem.

$$\begin{aligned}\frac{\partial^2 \mathcal{P}_{\mathrm{out},b}^{\mathrm{asym}}}{\partial \alpha^2} = & \frac{1}{(\alpha-\varphi_b\left(1-\alpha+k^2\right))}\frac{1}{\Gamma[m_{at}N_a]\Gamma[m_{tb}N_b]}\mathrm{e}^{-\frac{m_{tb}}{\Omega_{tb}}\frac{\epsilon_b}{P_{\mathrm{th}}}}\left(1+\varphi_b\right)^2 \\ & \times\left(\left(1+m_{tb}N_b-\frac{m_{tb}}{\Omega_{tb}}\frac{\epsilon_b}{P_{\mathrm{th}}}\right)\left(\frac{m_{tb}}{\Omega_{tb}}\frac{\epsilon_b}{P_{\mathrm{th}}}\right)^{m_{tb}N_b}+\frac{1}{m_{at}N_a}\left(\frac{m_{at}}{\Omega_{at}}\right)^{m_{at}N_a}\right. \\ & \times\left(\left(\frac{P_{\mathrm{th}}}{P_a}\right)^{m_{at}N_a}\left(1+m_{tb}N_b-\frac{m_{tb}}{\Omega_{tb}}\frac{\epsilon_b}{P_{\mathrm{th}}}\right)\left(\frac{m_{tb}}{\Omega_{tb}}\frac{\epsilon_b}{P_{\mathrm{th}}}\right)^{m_{tb}N_b}-\left(\frac{m_{tb}}{\Omega_{tb}}\right)^{m_{tb}N_b}\right. \\ & \times\left(\frac{\epsilon_b}{P_a}\right)^{m_{at}N_a}\left(\frac{\epsilon_b}{P_{\mathrm{th}}}\right)^{m_{tb}N_b-m_{at}N_a}\left(m_{tb}N_b-3m_{at}N_a-3\right)+\mathrm{e}^{\frac{m_{tb}}{\Omega_{tb}}\frac{\epsilon_b}{P_{\mathrm{th}}}} \\ & \left.\left.\times\ m_{at}N_a\left(\frac{m_{tb}}{\Omega_{tb}}\right)^{m_{at}N_a}\left(\frac{\epsilon_b}{P_a}\right)^{m_{at}N_a}\left(1+m_{at}N_a\right)\Gamma\left[m_{tb}N_b-m_{at}N_a,\frac{m_{tb}}{\Omega_{tb}}\frac{\epsilon_b}{P_{\mathrm{th}}}\right]\right)\right).\end{aligned} \tag{C.3}$$

$$\begin{aligned}\frac{\partial^2 \mathcal{P}_{\mathrm{out},b}^{\mathrm{asym}}}{\partial \alpha\partial \beta} = & \frac{1}{(\alpha-\varphi_b\left(1-\alpha+k^2\right))}\frac{1}{\beta}\frac{1}{\Gamma[m_{at}N_a]\Gamma[m_{tb}N_b]}\mathrm{e}^{-\frac{m_{tb}}{\Omega_{tb}}\frac{\epsilon_b}{P_{\mathrm{th}}}}\left(1+\varphi_b\right) \\ & \times\left(\left(m_{tb}N_b-\frac{m_{tb}}{\Omega_{tb}}\frac{\epsilon_b}{P_{\mathrm{th}}}\right)\left(\frac{m_{tb}}{\Omega_{tb}}\frac{\epsilon_b}{P_{\mathrm{th}}}\right)^{m_{tb}N_b}+\frac{1}{m_{at}N_a}\left(\frac{m_{at}}{\Omega_{at}}\right)^{m_{at}N_a}\right. \\ & \times\left(\left(\frac{P_{\mathrm{th}}}{P_a}\right)^{m_{at}N_a}\left(m_{tb}N_b-\frac{m_{tb}}{\Omega_{tb}}\frac{\epsilon_b}{P_{\mathrm{th}}}\right)\left(\frac{m_{tb}}{\Omega_{tb}}\frac{\epsilon_b}{P_{\mathrm{th}}}\right)^{m_{tb}N_b}\right. \\ & -\left(m_{tb}N_b-3m_{at}N_a+\frac{m_{tb}}{\Omega_{tb}}\frac{\epsilon_b}{P_{\mathrm{th}}}-2\right)\left(\frac{m_{tb}}{\Omega_{tb}}\right)^{m_{tb}N_b}\left(\frac{\epsilon_b}{P_a}\right)^{m_{at}N_a}\left(\frac{\epsilon_b}{P_{\mathrm{th}}}\right)^{m_{tb}N_b-m_{at}N_a} \\ & \left.\left.+\mathrm{e}^{\frac{m_{tb}}{\Omega_{tb}}\frac{\epsilon_b}{P_{\mathrm{th}}}}\left(m_{at}N_a\right)^2\left(\frac{m_{tb}}{\Omega_{tb}}\right)^{m_{at}N_a}\left(\frac{\epsilon_b}{P_a}\right)^{m_{at}N_a}\Gamma\left[m_{tb}N_b-m_{at}N_a,\frac{m_{tb}}{\Omega_{tb}}\frac{\epsilon_b}{P_{\mathrm{th}}}\right]\right)\right).\end{aligned} \tag{C.4}$$

$$\frac{\partial^2 \mathcal{P}_{\mathrm{out},b}^{\mathrm{asym}}}{\partial \beta^2} = \frac{1}{\beta^2} \frac{1}{\Gamma[m_{at}N_a]\Gamma[m_{tb}N_b]} \mathrm{e}^{-\frac{m_{tb}}{\Omega_{tb}}\frac{\epsilon_b}{P_{\mathrm{th}}}} \left(\left(1 + m_{tb}N_b - \frac{m_{tb}}{\Omega_{tb}}\frac{\epsilon_b}{P_{\mathrm{th}}} \right) \left(\frac{m_{tb}}{\Omega_{tb}}\frac{\epsilon_b}{P_{\mathrm{th}}} \right)^{m_{tb}N_b} \right.$$
$$+ \frac{1}{m_{at}N_a} \left(\frac{m_{at}}{\Omega_{at}} \right)^{m_{at}N_a} \left(\left(\frac{P_{\mathrm{th}}}{P_a} \right)^{m_{at}N_a} \left(1 + m_{tb}N_b - \frac{m_{tb}}{\Omega_{tb}}\frac{\epsilon_b}{P_{\mathrm{th}}} \right) \left(\frac{m_{tb}}{\Omega_{tb}}\frac{\epsilon_b}{P_{\mathrm{th}}} \right)^{m_{tb}N_b} \right.$$
$$- \left(m_{tb}N_b - m_{at}N_a - 3 - 2m_{at}N_a \mathrm{e}^{\frac{m_{tb}}{\Omega_{tb}}\frac{\epsilon_b}{P_{\mathrm{th}}}} \right) \left(\frac{m_{tb}}{\Omega_{tb}} \right)^{m_{tb}N_b} \left(\frac{\epsilon_b}{P_a} \right)^{m_{at}N_a} \left(\frac{\epsilon_b}{P_{\mathrm{th}}} \right)^{m_{tb}N_b - m_{at}N_a}$$
$$\left. \left. + \mathrm{e}^{\frac{m_{tb}}{\Omega_{tb}}\frac{\epsilon_b}{P_{\mathrm{th}}}} m_{at}N_a(1 + m_{at}N_a) \left(\frac{m_{tb}}{\Omega_{tb}} \right)^{m_{at}N_a} \left(\frac{\epsilon_b}{P_a} \right)^{m_{at}N_a} \Gamma \left[m_{tb}N_b - m_{at}N_a, \frac{m_{tb}}{\Omega_{tb}}\frac{\epsilon_b}{P_{\mathrm{th}}} \right] \right) \right). \tag{C.5}$$

References

[1] A. A. Khan, M. H. Rehmani, A. Rachedi, Cognitive-radio-based Internet of things: Applications, architectures, spectrum related functionalities, and future research directions, IEEE Wireless Commun. 24 (3) (2017) 17–25. doi:10.1109/MWC.2017.1600404.

[2] A. Goldsmith, S. A. Jafar, I. Maric, S. Srinivasa, Breaking spectrum gridlock with cognitive radios: An information theoretic perspective, Proc. IEEE 97 (5) (2009) 894–914. doi:10.1109/JPROC.2009.2015717.

[3] T. D. Ponnimbaduge Perera, D. N. K. Jayakody, S. K. Sharma, S. Chatzinotas, J. Li, Simultaneous wireless information and power transfer (SWIPT): Recent advances and future challenges, IEEE Commun. Surveys Tuts. 20 (1) (2018) 264–302. doi:10.1109/COMST.2017.2783901.

[4] X. Zhou, R. Zhang, C. K. Ho, Wireless information and power transfer: Architecture design and rate-energy tradeoff, IEEE Trans. Commun. 61 (11) (2013) 4754–4767. doi:10.1109/TCOMM.2013.13.120855.

[5] I. Krikidis, S. Timotheou, S. Nikolaou, G. Zheng, D. W. K. Ng, R. Schober, Simultaneous wireless information and power transfer in modern communication systems, IEEE Commun. Mag. 52 (11) (2014) 104–110. doi:10.1109/MCOM.2014.6957150.

[6] Y. Gu, S. Aïssa, RF-based energy harvesting in decode-and-forward relaying systems: Ergodic and outage capacities, IEEE Trans. Wireless Commun. 14 (11) (2015) 6425–6434. doi:10.1109/TWC.2015.2453418.

[7] Y. Dong, M. J. Hossain, J. Cheng, Performance of wireless powered amplify and forward relaying over Nakagami-m fading channels with nonlinear energy harvester, IEEE Commun. Lett. 20 (4) (2016) 672–675. doi:10.1109/LCOMM.2016.2528260.

[8] J. Laneman, D. Tse, G. Wornell, Cooperative diversity in wireless networks: Efficient protocols and outage behavior, IEEE Trans. Inf. Theory 50 (12) (2004) 3062–3080. doi:10.1109/TIT.2004.838089.

[9] O. Bazan, M. Jaseemuddin, A survey on MAC protocols for wireless adhoc networks with beamforming antennas, IEEE Commun. Surveys Tuts. 14 (2) (2012) 216–239. doi:10.1109/SURV.2011.041311.00099.

[10] E. Bjornson, M. Matthaiou, M. Debbah, A new look at dual-hop relaying: Performance limits with hardware impairments, IEEE Trans. Commun. 61 (11) (2013) 4512–4525. doi:10.1109/TCOMM.2013.100913.130282.

[11] C. Zhai, J. Liu, L. Zheng, Relay-based spectrum sharing with secondary users powered by wireless energy harvesting, IEEE Trans. Commun. 64 (5) (2016) 1875–1887. doi:10.1109/TCOMM.2016.2542822.

[12] D. K. Verma, R. Y. Chang, F.-T. Chien, Energy-assisted decode-and-forward for energy harvesting cooperative cognitive networks, IEEE Trans. Cognit. Commun. Netw. 3 (3) (2017) 328–342. doi:10.1109/TCCN.2017.2709759.

[13] D. S. Gurjar, H. H. Nguyen, H. D. Tuan, Wireless information and power transfer forIoT applications in overlay cognitive radio networks, IEEE Internet Things J. 6 (2) (2019) 3257–3270. doi:10.1109/JIOT.2018.2882207.

[14] F. Benkhelifa, M.-S. Alouini, Prioritizing data/energy thresholding-based antenna switching for SWIPT-enabled secondary receiver in cognitive radio

networks, IEEE Trans. Cognit. Commun. Netw. 3 (4) (2017) 782–800. doi:10.1109/TCCN.2017.2779478.

[15] J. Yan, Y. Liu, A dynamic swipt approach for cooperative cognitive radio networks, IEEE Trans. Veh. Technol. 66 (12) (2017) 11122–11136. doi:10.1109/TVT.2017.2734966.

[16] S. T. Shah, K. W. Choi, T.-J. Lee, M. Y. Chung, Outage probability and throughput analysis of SWIPT enabled cognitive relay network with ambient backscatter, IEEE Internet Things J. 5 (4) (2018) 3198–3208. doi:10.1109/JIOT.2018.2837120.

[17] Z. Yang, Z. Ding, P. Fan, G. K. Karagiannidis, Outage performance of cognitive relay networks with wireless information and power transfer, IEEE Trans. Veh. Technol. 65 (5) (2016) 3828–3833. doi:10.1109/TVT.2015.2443875.

[18] F. Zhou, N. C. Beaulieu, J. Cheng, Z. Chu, Y. Wang, Robust max–min fairness resource allocation in sensing-based wideband cognitive radio with SWIPT: Imperfect channel sensing, IEEE Systems J. 12 (3) (2018) 2361–2372. doi:10.1109/JSYST.2017.2698502.

[19] A. Mukherjee, T. Acharya, M. R. A. Khandaker, Outage analysis for SWIPT-enabled two-way cognitive cooperative communications, IEEE Trans. Veh. Technol. 67 (9) (2018) 9032–9036. doi:10.1109/TVT.2018.2840140.

[20] Z. Zhang, Y. Lu, Y. Huang, P. Zhang, Neural network-based relay selection in two-way SWIPT-enabled cognitive radio networks, IEEE Trans. Veh. Technol. 69 (6) (2020) 6264–6274. doi:10.1109/TVT.2020.2984327.

[21] M. Sun, M. Jin, Q. Guo, Y. Li, Throughput maximization for cognitive radio with wirelessly powered primary users, IEEE Syst. J. 14 (2) (2020) 2432–2442. doi:10.1109/JSYST.2019.2935263.

[22] S. Singh, D. Mitra, R. K. Baghel, Wireless powered communication network optimization using PSO-CS algorithm, Wireless Netw. 27 (2021) 4151–4167. doi:10.1007/s11276-021-02679-y.

[23] H. Bastami, M. Moradikia, H. Behroozi, R. C. de Lamare, A. Abdelhadi, Z. Ding, Secrecy rate maximization for hardware impaired untrusted relaying network with deep learning, Physical Communication 49 (2021) 101476. doi:10.1016/j.phycom.2021.101476.

[24] S. Fu, P. Jiang, C. Ding, Wireless powered hybrid backscatter-active communications with hardware impairments, Physical Communication 52 (2022) 101604. doi:10.1016/j.phycom.2022.1016046.

[25] Y. Alsaba, S. K. A. Rahim, C. Y. Leow, Beamforming in wireless energy harvesting communications systems: A survey, IEEE Commun. Surveys Tuts. 20 (2) (2018) 1329–1360. doi:10.1109/COMST.2018.2797886.

[26] R. Manna, R. H. Y. Louie, Y. Li, B. Vucetic, Cooperative spectrum sharing in cognitive radio networks with multiple antennas, IEEE Trans. Signal Proces. 59 (11) (2011) 5509–5522. doi:10.1109/TSP.2011.2163068.

[27] Y. Cao, C. Tellambura, Cognitive beamforming in underlay two-way relay networks with multiantenna terminals, IEEE Trans. Cognit. Commun. Netw. 1 (3) (2015) 294–304. doi:10.1109/TCCN.2015.2498615.

[28] P. V. Tuan, I. Koo, Optimal multiuser MISO beamforming for power-splitting SWIPT cognitive radio networks, IEEE Access 5 (2017) 14141–14153. doi:10.1109/ACCESS.2017.2727073.

[29] F. Zhou, Z. Li, J. Cheng, Q. Li, J. Si, Robust AN-aided beamforming and power splitting design for secure MISO cognitive radio with SWIPT, IEEE Trans. Wireless Commun. 16 (4) (2017) 2450–2464. doi:10.1109/TWC.2017.2665465.

[30] L. Mohjazi, I. Ahmed, S. Muhaidat, M. Dianati, M. Al-Qutayri, Downlink beamforming for SWIPT multi-user MISO underlay cognitive radio net-

works, IEEE Commun. Lett. 21 (2) (2017) 434–437. doi:10.1109/LCOMM.2016.2619340.

[31] D. S. Gurjar, P. K. Upadhyay, D. B. da Costa, R. T. de Sousa, Beamforming in traffic-aware two-way relay systems with channel estimation error and feedback delay, IEEE Trans. Veh. Technol. 66 (10) (2017) 8807–8820. doi:10.1109/TVT.2017.2696047.

[32] E. Fidan, O. Kucur, Performance of transceiver antenna selection in two way full-duplex relay networks over Rayleigh fading channels, IEEE Trans. Veh. Technol. 67 (7) (2018) 5909–5921. doi:10.1109/TVT.2018.2803280.

[33] M. Zhang, Y. Liu, Secure beamforming for untrusted MISO cognitive radio networks, IEEE Trans. Wireless Commun. 17 (7) (2018) 4861–4872. doi:10.1109/TWC.2018.2832214.

[34] S. Benmahmoud, H. Dai, A unified framework for the performance evaluation of single-branch dual-hop AF relaying in the presence of transceiver hardware impairments, Phys. Commun. 32 (2019) 231–241. doi:https://doi.org/10.1016/j.phycom.2018.12.008.

[35] P. Kharwar, S. Yadav, N. Purohit, Optimal power allocation for the multiple-sensor single-DF relay based IoT networks under transceiver hardware impairments, Phys. Commun. 43 (2020) 101183. doi:https://doi.org/10.1016/j.phycom.2020.101183.

[36] M. Ucar-Gul, M. NAMDAR, A. Basgumus, Performance analysis of two-way AF relaying system with the presence of hardware impairments over nakagami-m fading channels, IET Communications 14. doi:10.1049/iet-com.2019.0839.

[37] M. Tian, W. Sun, L. Huang, S. Zhao, Q. Li, Joint beamforming and relay selection in AF two-way relay networks with energy transfer, IEEE Systems J. 14 (2) (2020) 2597–2600. doi:10.1109/JSYST.2019.2933162.

[38] Q. Li, L. Yang, Beamforming for cooperative secure transmission in cognitive two-way relay networks, IEEE Trans. Inf. Forensics Security 15 (2020) 130–143. doi:10.1109/TIFS.2019.2918431.

[39] I. S. Gradshteyn, I. M. Ryshik, Table of integrals, series, and products, New York, NY, USA: Academic 7th ed.

[40] J. Zan, G. Lu, Y. Ye, Outage performance of UAV-assisted AF relaying with hardware impairments, Phys. Commun. 46 (2021) 101334. doi:https://doi.org/10.1016/j.phycom.2021.101334.

[41] S. Solanki, V. Singh, P. K. Upadhyay, RF energy harvesting in hybrid two-way relaying systems with hardware impairments, IEEE Trans. Veh. Technol. 68 (12) (2019) 11792–11805. doi:10.1109/TVT.2019.2944248.

[42] D. S. Gurjar, P. K. Upadhyay, D. B. da Costa, R. T. de Sousa, Beamforming in traffic-aware two-way relay systems with channel estimation error and feedback delay, IEEE Trans. Veh. Technol. 66 (10) (2017) 8807–8820. doi:10.1109/TVT.2017.2696047.

[43] N. Jain, V. A. Bohara, Energy harvesting and spectrum sharing protocol for wireless sensor networks, IEEE Wireless Commun. Lett. 4 (6) (2015) 697–700. doi:10.1109/LWC.2015.2484341.

[44] D. N. K. Jayakody, T. D. P. Perera, A. Ghrayeb, M. O. Hasna, Self-energized UAV-assisted scheme for cooperative wireless relay networks, IEEE Trans. Veh. Technol. 69 (1) (2020) 578–592. doi:10.1109/TVT.2019.2950041.

[45] A. Sarthi, D. S. Gurjar, C. Sai, P. Pattanayak, A. Bhardwaj, Performance impact of hardware impairments on wireless powered cognitive radio sensor networks, IEEE Sensors Lett. 4 (6) (2020) 1–4. doi:10.1109/LSENS.2020.2994595.

[46] S. Yadav, D. S. Gurjar, Physical layer security in underlay cognitive radio networks over α-μ fading channels, in: 2020 IEEE Latin-American Con-

ference on Communications (LATINCOM), 2020, pp. 1–6. doi:10.1109/LATINCOM50620.2020.9282325.

[47] H. Lee, C. Song, S.-H. Choi, I. Lee, Outage probability analysis and power splitter designs for SWIPT relaying systems with direct link, IEEE Commun. Lett. 21 (3) (2017) 648–651. doi:10.1109/LCOMM.2016.2627055.